PCCP

PAPER

View Article Online
View Journal | View Issue

Cite this: *Phys. Chem. Chem. Phys.*, 2022, **24**, 3722

Structural study of 1- and 2-naphthol: new insights into the non-covalent H–H interaction in *cis*-1-naphthol†

Arsh S. Hazrah, [a] Sadisha Nanayakkara, [b] Nathan A. Seifert,‡[a] Elfi Kraka [b] and Wolfgang Jäger *[a]

Received 10th December 2021,
Accepted 18th January 2022

DOI: 10.1039/d1cp05632h

rsc.li/pccp

Previous microwave studies of naphthol monomers were supplemented by measuring spectra of all ^{13}C mono-substituted isotopologues of the *cis*- and *trans*-conformers of 1-naphthol and 2-naphthol in their natural abundances. The resulting data were utilized to determine substitution structures and so-called semi-experimental effective structures. Results from electronic structure calculations show that the OH group of *cis*-1-naphthol points $\approx 6^\circ$ out of plane, which is consistent with the inertial defect data of *cis*- and *trans*-1-naphthol. The non-planarity of *cis*-1-naphthol is a result of a close-contact H-atom–H-atom interaction. This type of H–H interaction has been the subject of much controversy in the past and we provide here an in-depth theoretical analysis of it. The naphthol system is particularly well-suited for such analysis as it provides internal standards with its four different isomers. The methods used include quantum theory of atoms in molecules, non-covalent interactions, independent gradient model, local vibrational mode, charge model 5, and natural bond orbital analyses. We demonstrate that the close-contact H–H interaction is neither a purely attractive nor repulsive interaction, but rather a mixture of the two.

Introduction

1- and 2-naphthol, hydroxy-derivatives of naphthalene, the simplest polycyclic aromatic hydrocarbon, are used as precursors in the dye, perfume, insecticide, and pharmaceutical industries[1] and are metabolites of naphthalene itself,[2] which has uses as pesticide.[3] Naphthols can also be considered as naphthalene homologues of phenol and are, from an intermolecular interactions point of view, of interest because they contain a hydrophobic part, *i.e.* the bicycle with an extended π-electron system, and a hydrophilic OH group.

Indeed, a number of weakly bound complexes involving the naphthols have been studied using spectroscopic techniques. The Leutwyler group in particular has studied 1-naphthol–$(H_2O)_N$ (N = 1 to 50)[4] and 2-naphthol–$(NH_3)_N$ (N = 1–10)[5] complexes and clusters with laser spectroscopic techniques in an effort to determine the solvation threshold for excited state proton transfer from naphthol to water, 1-naphthol–alkane complexes,[6–8] 1-naphthol–rare gas and N_2 complexes,[9] hydrogen-bonded complexes of naphthol,[10–12] and most recently complexes of 1-naphthol with linear molecules.[13] Naphthol–water clusters have also been studied by the Fujii group,[14] by Knochenmuss and Smith,[15] and by Pratt *et al.*[16] The 1-naphthol dimer has been studied by infrared dip spectroscopy[17] and more recently the microwave spectrum of the 1-naphthol dimer has been measured, assigned, and interpreted, with the help of theoretical calculations, in terms of a structure that is dominated by π–π stacking interactions over canonical hydrogen bonding.[18]

There are a number of earlier spectroscopic studies of the naphthol monomers. Pratt's group has studied the fluorescence spectra of 1- and 2-naphthol[19] and established the existence of *cis*- and *trans*-conformers for both monomers. This was followed by a microwave spectroscopic study of *cis*- and *trans*-1-naphthol by Brown and co-workers,[20] who identified a close contact between the hydroxyl H and the neighbouring ring H-atom. Saeki *et al.*[17] reported then on infrared dip spectra of *trans*- and *cis*-1-naphthol. Recently, Goubet *et al.*[21] measured rotational

[a] *Department of Chemistry, University of Alberta, Edmonton, Alberta, T6G 2G2, Canada. E-mail: wolfgang.jaeger@ualberta.ca*
[b] *Department of Chemistry, Southern Methodist University, Dallas, TX, 75275-0314, USA. E-mail: ekraka@smu.edu*

† Electronic supplementary information (ESI) available: Measured transition frequencies, derived spectroscopic constants, structural parameters, results from QTAIM analyses, results from local mode analyses, results from charge model 5 analysis, and results from natural bond orbital analysis. See DOI: 10.1039/d1cp05632h

‡ Current address: Department of Chemistry and Chemical & Biomedical Engineering, University of New Haven, 300 Boston Post Road, West Haven, CT 06516, USA.

and vibrational spectra of *cis*-2-naphthol and re-examined the spectra of *trans*-1-naphthol.

Close H–H contacts of the type identified by Brown and co-workers in *cis*-1-naphthol have been found also in other systems. Analysis and characterization of these close H–H contacts has attracted considerable attention in the past two decades or so. Bader and co-workers[22–24] examined close-contact H–H interactions in several crystal structures and isolated polycyclic aromatic hydrocarbons. They found, within the framework of the quantum theory of atoms in molecules (QTAIM), a bond critical point between close-contact hydrogen atoms indicative of a bonding interaction. The authors ultimately conclude that these close-contact H–H interactions are attractive interactions which help stabilize the overall structure of the crystal or molecule. This conclusion has, however, been contested in several other studies[25–27] which argue that close-contact H–H interactions are indeed repulsive or steric interactions. For example, Grimme *et al.*[26] showed experimentally that the steric congestion of the close-contact hydrogens results in shorter C–H bond lengths, indicated by a vibrational blue shift, which aligns with the traditional view of steric repulsion. The studies discussed focus on molecules or systems where the close-contact hydrogens are ''fixed'' in place where the two hydrogens are forced to interact with each other. This is not the case with the naphthol monomers where the hydroxyl hydrogen is not locked into position like the C–H hydrogens considered in previous studies. *cis*-1-naphthol thus provides an interesting test case to analyze the close-contact H–H interaction in detail, where the other isomers can play the role of internal references. What makes 1-naphthol even more suited is that it affords us the opportunity to computationally follow electronic properties along the smooth OH internal rotation coordinate from the close H–H contact *cis*-conformer to the *trans*-conformer.

Here, we describe the rotational spectrum of *trans*-2-naphthol measured with a chirped-pulse Fourier transform microwave spectrometer in the 2 to 6 GHz range. Spectra of all singly substituted ^{13}C isotopologues were also recorded, in addition to those of *cis*- and *trans*-1-naphthol and *cis*-2-naphthol. The isotopic data were used to derive heavy atom Kraitchman substitution coordinates[28] and semi-experimental structures for both conformers of both isomers. The close H–H contact in *cis*-1-naphthol is a main focus of this study. A Quantum Theory of Atoms-in-Molecules (QTAIM)[29] analysis revealed a bond critical point between the two hydrogen atoms and a Non-Covalent Interactions (NCI) analysis[30] resulted in a reduced electron density gradient isosurface with positive sign of the second Hessian eigenvalue, which is often an indication for an attractive interaction. We applied several approaches to provide further insights into the weak intramolecular interactions within each conformer. The electron density topology was also analyzed using the Independent Gradient Model (IGM)[31–33] to extract the Intrinsic Bond Strength Index (IBSI)[34] for relevant individual bonds in 1-naphthol. The local vibrational mode theory[35] originally introduced by Konkoli, Cremer *et al.*[36–40] was utilized to assess and compare the intrinsic strength of the OH bond in both isomers of 1- and 2-naphthol. Finally, we also used Charge Model 5 (CM5)[41] and Natural Bond Orbitals (NBO)[42,43] approaches to gain further insights into the close-contact H–H interaction.

Close-contact H–H interactions of the type observed in *cis*-1-naphthol have been extensively and controversially discussed in the literature. A main purpose of the analyses applied here to the naphthol isomers is to arrive at a consistent and convincing physical–chemical picture of such close-contact H–H interactions.

Materials and methods

Theoretical methods

Utilizing density functional theory (DFT)[44] and the Gaussian 16 program suite,[45] geometry optimizations and harmonic frequency calculations were performed at the B3LYP-D3(BJ)[46–48] level of theory with the def2-TZVP basis set[49] and at the Møller–Plesset second order perturbation theory (MP2)[50] level with the aug-cc-pVTZ basis set.

Analyses of the molecular electron density distribution based on Bader's quantum theory of atoms in molecules (QTAIM),[29] including non-covalent interactions (NCI)[30] and IGM analyses,[31–33] were done using the AIMAll,[51] MultiWfn,[52] and IGMPlot programs, respectively, and then visualized using UCSF Chimera.[53] The local mode analyses were carried out with the program LModeA.[54]

Normal vibrational modes are generally delocalized as a result of mass coupling.[55] This implies that if one considers a particular normal stretching mode between two atoms of interest, it can be coupled to other normal modes such as bending or torsion, which hampers the direct correlation between stretching frequency and bond strength as well as the comparison between stretching modes of similar nature. As a consequence, the normal stretching force constant cannot be used as a direct bond strength measure, which results in the need to derive a local counterpart that is free from any mode-mode coupling. Konkoli, Cremer *et al.*[36–40] approached this problem by solving the mass-decoupled analogue of Wilson's equation of vibrational spectroscopy[55] leading to local vibrational modes, associated local mode frequencies, and local mode force constants. Zou and Cremer showed that the local stretching force constant reflects the curvature of the PES in the direction of the bond stretching.[56] This important result qualifies the local stretching force constants k^a as a unique quantitative measure of the intrinsic strength of a chemical bond and/or weak chemical interaction based on vibrational spectroscopy, which has been extensively applied in previous work.[35] (For some recent work see also ref. 57–60). Another important feature of the local vibrational mode theory is that any complete set of non-redundant local modes can be transformed into the corresponding set of normal modes *via* an adiabatic connection scheme.[61] This unique one-to-one correspondence has led to a new comprehensive analysis of infrared/Raman spectra *via* the characterization of normal modes (CNM) procedure[38,62] which allows for the decomposition of each normal

mode into its respective local mode counterparts, thereby facilitating the identification of their individual contributions. The local mode analysis (LMA) was applied in this work to assess the strength of the O–H bonds in *cis*- and *trans*-1- and 2-naphthol and to evaluate the local character of the corresponding O–H normal modes. For convenience, k^a values were converted into more chemically intuitive bond strength orders (BSO n) by utilizing an extended Badger rule.[39,63] The latter relates BSO n to k^a *via* a power relationship, which is fully determined based on two well-known reference molecules and the requirement that for a zero-force constant, the corresponding BSO n is zero:

$$\text{BSO } n = a(k^a)^b \quad (1)$$

In this work, the constants a and b were evaluated using F–H and $[F\cdots H\cdots F]^-$ as the references with BSO n values 1 and 0.5, respectively, which resulted in a = 0.518 (0.490) and b = 0.291 (0.319) (values for MP2/aug-cc-pVTZ calculations are shown first, followed by those of B3LYP-D3(BJ)/def2-TZVP calculations in parentheses). The corresponding k^a values for F–H and $[F\cdots H\cdots F]^-$ are 9.584 (9.367) mDyn Å^{-1} and 0.884 (1.064) mDyn Å^{-1}, respectively. Since we are interested in O–H bonds, we scaled the BSO n values obtained *via* eqn (1), according to which the O–H bond in H_2O has BSO n values of 0.961 (0.957) by a factor of 1.041 (1.045), so that BSO n OH in H_2O is 1.

Experimental methods

Rotational spectra of the naphthols were recorded with a pulsed nozzle chirped-pulse Fourier transform spectrometer in the frequency range between 2 and 6 GHz. Our instrument operates analogously to the spectrometer designed by the Pate group,[64] with some variances in component specifications.[65] Per molecular pulse, we recorded six free induction decays (FIDs). About 3.8 M (850 k) FIDs were averaged and then Fourier transformed to generate the broadband rotational spectrum for 1-naphthol (2-naphthol). 3.8 M averages were necessary to measure ^{13}C transition for the *cis*-1-naphthol conformer with sufficient signal to noise ratio.

The 1- and 2-naphthol ($\geq$99%) samples were purchased from Millipore-Sigma and used without any further modification or purification. Both 1- and 2-naphthol are solids with melting points of about 95 and 120 °C, respectively. To generate the vapour pressure needed to bring a sufficient number of molecules into the gas phase, we utilized a special attachment to a General Valve, Series 9, pulsed valve which contains a sample reservoir and can be heated. For 1-naphthol the attachment was heated to 100 °C and for 2-naphthol to 120 °C. Neon (helium) was used as backing gas at pressures of about 3 atm for 1-naphthol (2-naphthol). Neon backing gas improved the signal to noise ratio for 1-naphthol and was used to measure its ^{13}C transitions.

Results and discussion

Experimental results

Sections of the broadband rotational spectra for 1-naphthol and 2-naphthol are shown in Fig. S1 of the ESI.† Rotational and centrifugal distortion constants from the literature[20,21] and from DFT calculations were used to locate the rotational transitions for the normal isotopologues of *cis*- and *trans*-conformers of 1-and 2-naphthol. The transition frequencies are in Tables S2–S4, ESI,† together with the quantum number assignments. The measured frequencies were used, together with those from the literature where available, in fitting procedures using the SPCAT/SPFIT program suite[66] and Watson's A-reduction Hamiltonian in its I^r representation to determine experimental rotational and quartic centrifugal distortion constants. The fit results for *trans*-1-naphthol are included in Table 1, while the fit results for *cis*-2-naphthol, *cis*- and *trans*-1-naphthol, with frequencies from earlier work included, are presented in Table S1 of the ESI.† The transitions were strong enough that all ten singly substituted ^{13}C isotopologues for both conformers of 1- and 2-naphthol could be detected in their natural abundances. The resulting transition frequencies with quantum number assignments are in Tables S6–S9 of the ESI† and the corresponding spectroscopic constants are given in Tables S10–S13 of the ESI.† For the normal isotopologues of *cis*- and *trans*-1-naphthol and *cis*-2-naphthol, the derived spectroscopic constants agree with the literature values to within the respective uncertainties.

Electronic structure calculations

Geometry optimizations and harmonic vibrational frequency calculations were performed at the B3LYP-D3(BJ)/def2-TZVP and MP2/aug-cc-pVTZ level for both *trans*- and *cis*-conformers of 1- and 2-naphthol. The resulting structural parameters are given in Tables S14–S17 of the ESI† and the corresponding rotational constants, centrifugal distortion constants, and dipole moment components are in Table 1 and Table S1, ESI;† the structures are shown in Fig. 1. The dihedral angles τ(C2–C1–O1–H1) for 1-naphthol and τ(C1–C2–O1–H2) for 2-naphthol were scanned to obtain potential energy curves (Fig. S2, ESI†) that connect the *trans*- to the *cis*-isomers *via* barriers of 13.6 kJ mol^{-1} (1-naphthol) and 12.8 kJ mol^{-1} (2-naphthol). At the B3LYP-D3(BJ)/def2-TZVP level of theory, the relative zero-point energy differences between the *trans*- and *cis*-isomers are 3.4 kJ mol^{-1}

Table 1 Spectroscopic parameters for *trans*-2-naphthol from theory and from fits of experimental data

	trans-2-naphthol (B3LYP-D3(BJ)/def2-TZVP)	*trans*-2-naphthol (Experiment)
A/MHz	2868.6589	2845.35720(37)
B	829.6421	825.53635(13)
C	643.5280	640.08718(16)
Δ_J/kHz	0.00793	0.0070(17)
Δ_{JK}	0.01508	[0.01508][a]
Δ_K	0.18328	0.261(17)
δ_J	0.00197	0.00180(92)
δ_K	0.02969	[0.02969][a]
N	—	49
σ/kHz	—	2.7
ΔE_0/kJ mol^{-1}	2.1	—
Δ/amu Å^2	0.0000	−0.251(1)
$\lvert\mu\rvert$/D	μ_a = 0.6, μ_b = 1.4, μ_c = 0.0	$\mu_b > \mu_a$

[a] Fixed to theory in the fit.

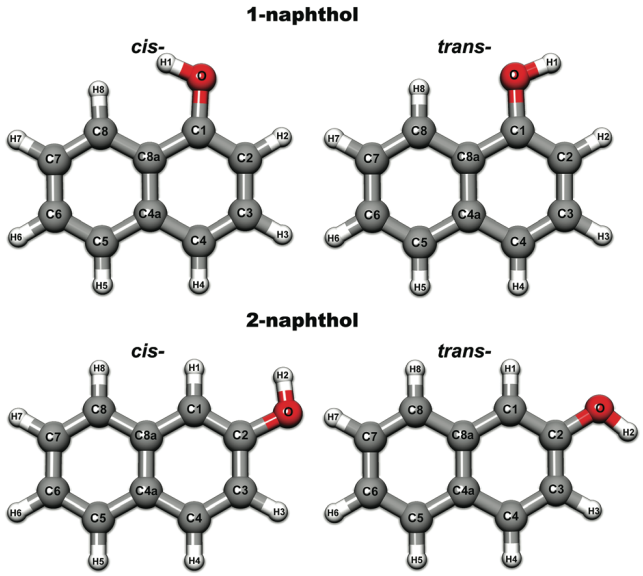

Fig. 1 Atom number labelling for all four isomers of naphthol.

(1-naphthol) and 1.9 kJ mol^{-1} (2-naphthol). In 1-naphthol, the *trans*-conformer is lower in energy, while in 2-naphthol the *cis*-conformer is the lower energy conformer. This ordering is consistent with previous determinations.[21,67,68]

To gain insights into the intramolecular interactions in the naphthol monomers, we performed QTAIM (Fig. 2), NCI (Fig. S3, ESI†), and IGM analyses of the molecular electron density distributions. Interestingly, we found, apart from the expected bond and ring critical points in the naphthol skeleton, a bond path with a bond critical point between the hydroxyl H-atom and the neighbouring H-atom at the adjacent ring in *cis*-1-naphthol (see Fig. 2) in the QTAIM analysis. Numerical results from these analyses are given in Table S18, ESI.† Additional electronic structure calculations were done at the ωB97XD[69]/Jun-cc-pVTZ[70] and, MP2/aug-cc-pVTZ levels of theory to confirm that the bond critical point and the numerical data from the QTAIM analyses are not unique to the B3LYP-D3(BJ)/def2-TZVP level of theory. The results of this comparison are shown in Table S19 of the ESI.†

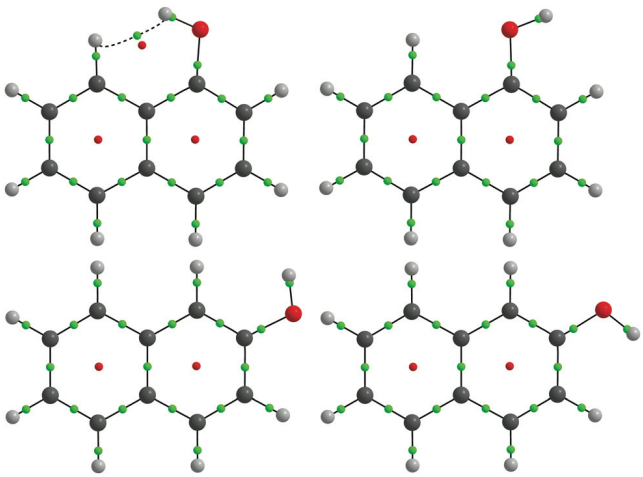

Fig. 2 Results from QTAIM analyses for the four experimentally observed isomers of naphthol. The green spheres denote bond critical points, while the red spheres denote ring critical points.

Structures

The experimental and theoretical (B3LYP-D3(BJ)/def2-TZVP level of theory) rotational constants for *cis*- and *trans*-isomers of both 1- and 2-naphthol in Table 1 and Table S1, ESI,† differ by at most 0.8%, which is indicative of reasonable agreement between theoretical structural parameters and those underlying the experimental rotational constants. For a meaningful comparison, however, one needs to take into account the effects of zero-point vibrational motions that cause the difference between equilibrium (r_e) structure and equilibrium (A_e, B_e, C_e) rotational constants on one hand and effective (r_o) structure and ground state (A_0, B_0, C_0) rotational constants on the other. The anharmonic vibrational contributions to the rotational constants were calculated using vibrational perturbation theory (VPT2) at the B3LYP-D3(BJ)/def2-TZVP level and subtracted from the experimental constants to arrive at the so-called semi-experimental rotational constants,[71–73] given in Table 2 and Tables S20–S24 in the ESI.† The largest difference to the theoretical equilibrium constants is now less than 0.1%.

To further assess the quality of the semi-experimental rotational constants, one may look at the inertial defects, defined as $\Delta_I = I_C - (I_A + I_B)$. For a planar rigid molecule Δ_I is zero. The inertial defects for the naphthol isomers (Table 1 and Table S1, ESI†) range from −0.212 to −0.293 amu Å^2 and are consistent with bicyclic heterocycles whose Δ_I values have been discussed in detail by Jahn *et al.*[74] The negative values are a result of greater contributions by out-of-plane zero-point vibrational motions to the inertial defect compared to the in-plane vibrations. The *cis*-1-naphthol isomer has the largest magnitude Δ_I value. The difference in Δ_I between *cis*- and *trans*-1-naphthol is −0.080 amu Å^2, in reasonable agreement with the theoretical value of Δ_I for *cis*-1-naphthol (−0.047 amu Å^2). The non-zero theoretical value of Δ_I for *cis*-1-naphthol is attributable to the out-of-plane location of the OH H-atom with a dihedral angle τ of 6°. The experimental difference between Δ_I values of 0.080 amu Å^2 corresponds to a dihedral angle τ of 10°. The Δ_I values calculated from the semi-experimental constants (Table S20, ESI†) are reduced by about 80% and have magnitudes on the order of 0.05 amu Å^2 or smaller. It is interesting to note that there is an overcorrection for Δ_I in *cis*-1-naphthol compared to the other isomers. This leads to a positive semi-experimental Δ_I value that is not consistent anymore with the out-of-plane OH H-atom in *cis*-1-naphthol. It is likely that the large amplitude motion of the OH H-atom from above to below the heavy atom plane in

Table 2 Experimental, semi-experimental, and theoretical rotational constants of *cis*-1-naphthol

Constant	Experiment	Semi-experimental	B3LYP-D3(BJ)
A/MHz	1947.51310	1962.355	1959.859
B/MHz	1124.30739	1130.679	1130.834
C/MHz	713.09734	717.334	717.128

cis-1-naphthol is not captured properly in the anharmonic calculations, thus leading to the inconsistency.

Additionally, we compare our inertial defect values to those discussed by Jahn *et al.*[74] to examine how naphthol compares to other heterocyclic molecules. The calculated values in Table S26, ESI,† for the four isomers of naphthol were computed by summing Oka's equation[75] over the lowest out-of-plane vibrations:

$$\Delta_{0l} = -\sum_{l=1}^{n} \frac{33.175}{\nu_l} \text{ amu Å}^2 \text{ cm}^{-1} \quad (2)$$

Oka noted that eqn (2) overestimates the magnitude of Δ_0 and introduced an empirical correction to compensate for this overcorrection:

$$\Delta_0 = \Delta_{0l} + \alpha\sqrt{I_{cc}} \quad (3)$$

Here, α is a unitless value used to describe the slope of eqn (3), and $\sqrt{I_{cc}}$ is the square root of the moment of inertia along the *c* principal inertial axis.

As outlined by Jahn *et al.* the number of out-of-plane modes used in the sum is equal to the number of rings present, or for molecules with an extra low wavenumber out-of-plane vibration (<100 cm^{-1}) is equal to the number of rings +1. The five lowest out-of-plane vibrations for all four isomers of naphthol, with their respective displacement vectors, are presented in Fig. S8–S11 (ESI†). Based on the results of Jahn *et al.*, for *trans*-1-naphthol and both isomers of 2-naphthol the two lowest out-of-plane vibrations should be used, while the three lowest out-of-plane vibrations should be used for *cis*-1-naphthol to account for the existence of an extra low wavenumber OH out-of-plane vibration. A plot showing the differences between the experimental inertial defect and calculated inertial defect values for different numbers of out-of-plane vibrational modes is shown in Fig. S12 (ESI†). The frequencies of the vibrational modes for each isomer were obtained from the B3LYP-D3(BJ)/def2-TZVP results. The calculated and experimental inertial defect values and the difference between the two are shown in Table S26 of the ESI.† The calculated inertial defect values from the five lowest out-of-plane modes and the difference between the calculated and experimental defects values are presented in Tables S27 and S28 of the ESI,† respectively. *cis*-1-naphthol has a difference of $\approx$0.49 amu Å^2 (three modes), while the differences for *trans*-1-naphthol and both isomers of 2-naphthol range from 0.21–0.23 amu Å^2 (two modes). Comparing these results to the Jahn *et al.* fit presented in Fig. S12 (ESI†), there is a discrepancy in the $\sqrt{I_{cc}}$ values determined from the plot using the inertial defect difference and the experimental $\sqrt{I_{cc}}$ values. For *trans*-1-naphthol the fit slightly underestimates the experimental $\sqrt{I_{cc}}$ value ($\approx$26.6 amu$^{1/2}$ Å) by several amu$^{1/2}$ Å when the two lowest out-of-plane vibrations are used in the sum. The fit also underestimates the experimental $\sqrt{I_{cc}}$ values for both isomers of 2-naphthol when the two lowest out-of-plane vibrations are used, where the averaged 28.1 amu$^{1/2}$ Å value does not correspond to an average inertial defect difference of 0.22 amu Å^2. The largest discrepancy between the fit data and our results are for *cis*-1-naphthol where the inertial difference of 0.49 amu Å^2 is severely overestimated by the fit of Jahn *et al.*, when the three lowest out-of-plane modes are used to account for the extra low wavenumber out-of-plane vibration. Using the two lowest out-of-plane vibrations instead of the three lowest, the difference (0.32 amu Å^2) becomes much closer to the fit of Jahn *et al.* One potential reason for the discrepancy may be the molecules selected by the authors to construct the fit, which does indeed contain a wider range of sizes of heterocyclic compounds, but do not have any conformational flexibility. Although the skeleton structure of naphthol is not flexible, the hydroxyl group does provide a degree of flexibility which most likely leads to the discrepancy between the result herein and the Jahn *et al.* fit.

The semi-experimental rotational constants of normal and singly substituted ^{13}C isotopologues of both conformers of 1- and 2-naphthol were used in a fitting procedure to produce the structural parameters in Tables S14–S17 of the ESI.† Comparison with the theoretical structure in the same tables shows, in general, good agreement with the average differences on the order of 0.04 Å and 0.9° for bond lengths and angles, respectively.

Another way to minimize the effects of zero-point vibrational motions on structural parameters that is purely based on experimental data is a Kraitchman substitution analysis.[28] Since rotational constants are available for all singly substituted ^{13}C isotopologues, we were able to produce substitution coordinates for all carbon atoms of *cis*- and *trans*- 1- and 2-naphthol. The resulting substitution, r_s, structural parameters are also in Tables S14–S17 of the ESI† and are in very good agreement with the theoretical and semi-experimental values. The largest differences are on the order of 0.03 Å and 2° for bond lengths and angles, respectively.

Interpretation of the close contact in *cis*-1-naphthol

The naphthol monomers are well suited to shed light on the nature of close-contact H–H interactions. A reason is the availability of the other isomers which can be utilized as internal standards. In this sense, *trans*-1-naphthol is particularly relevant because of the relatively shallow conversion pathway to *cis*-1-naphthol, which allowed us to map relevant properties smoothly from a close-contact H–H interaction to the absence of such interaction (*vide infra*). Interpretation of the nature of the H–H close contact in *cis*-1-naphthol was done *via* several approaches: (a) atomic energies from QTAIM and NCI plots; (b) IGM analysis; (c) local mode analysis; (d) CM5 atomic charge analysis; (e) NBO analysis (electron occupancy, stabilization energies, and steric exchange energies). *trans*-1-naphthol, *cis*-2-naphthol, and *trans*-2-naphthol were used as control molecules.

(a) QTAIM and NCI results. The bond path between the close-contact hydrogen atoms and the corresponding bond critical point found in the QTAIM analysis of *cis*-1-naphthol appears to be indicating a bonding interaction between those two H-atoms. This is in stark contrast with the traditional notion of a steric repulsion at a separation of only 1.9 Å, much shorter than the sum of the van der Waals radii of $\approx$2.4 Å. Accompanying the H–H bond critical point is a ring critical

point that is associated with the 6-ring formed by the H–H interaction, in accord with the Poincaré–Hopf relationship. One can follow the evolution of these two critical points along the *cis–trans* conversion coordinate and finds that they coalesce and disappear if the dihedral angle τ becomes greater than 21°. Similar effects have been found by the Bader group in pure hydrocarbons, such as phenanthrene,[22] where the two close-contact H-atoms are also connected by a bond path with a bond critical point. This apparent bonding interaction between two equally or similarly charged hydrogen atoms was termed hydrogen–hydrogen, or H–H, bonding, in contrast to dihydrogen bonding, where the two interacting H-atoms have a charge difference of about 1 *e* or more.[22] Bader and co-workers have considered atomic energies within the framework of QTAIM to rationalize the existence of H–H bonding. The atomic energies are obtained by partitioning the molecular kinetic electronic energy among the atomic basins whose extents are defined by the topology of the electron density. Bader and co-workers note that the presence of the H–H bond path is accompanied by a lowering of the collective H-atom energy, in the case of phenanthrene *versus* its linear isomer anthracene, for example. The concurrent increase in carbon skeleton energy is less in magnitude, such that overall phenanthrene is lower in energy than anthracene.

In some of the hydrocarbons considered by Bader and co-workers, the H-atoms are forced into close contact by the rigid structure of the C-atom skeletons. The case of *cis*-1-naphthol is interesting because of the flexibility in the OH-group orientation; the close H–H contact is adopted 'voluntarily'. We carried out analyses analogous to those by Bader and co-workers for *cis*- and *trans*-1-naphthol using the AIMAll program. A compilation of relevant data from these analyses is given in Table S18 of the ESI.† It has been asserted before that the electron density distribution is rather insensitive to the level of theory employed,[30,76] so that, for larger systems, even the use of promolecular densities is suggested for electron density analyses. (See, however, also, for example, Joubert *et al.*[77]) Nevertheless, to make sure that the analyses and conclusions drawn are not an artifact of the level of theory employed, we did calculations also at the ωB97XD/Jun-cc-pVTZ and MP2/aug-cc-pVTZ levels of theory for *cis*-1-naphthol. The results are in excellent agreement with those from the B3LYP-D3(BJ)/def2-TZVP calculations (seen Table S19, ESI†), confirming the level of theory has relatively small effect on the molecular electron density distribution.

Properties of the H–H bond critical point and the newly formed ring critical point are in accord with those of other systems with H–H close contacts.[22] For example, the H–H bond critical point is characterized by a low value of 0.015 a.u. for ρ, the electron density, a small positive value of 0.058 a.u. for $\nabla^2\rho$, the Laplacian of the electron density, an energy density H, of 0.0025 a.u., and a relatively large value of 1.1 for the bond ellipticity, ε. For comparison, the values for the bond critical point of the strong hydrogen bonding interaction in the water dimer are: ρ = 0.026 a.u., $\nabla^2\rho$ = 0.090 a.u., H = 0.00098 a.u., ε = 0.025 at the B3LYP-D3(BJ)/def2-TZVP level of theory. For the acyclic formic acid dimer, the strong hydrogen bond has values of ρ = 0.033 a.u., $\nabla^2\rho$ = 0.114 a.u., H = 0.000094 a.u., ε = 0.033 and the weaker hydrogen bond ρ = 0.011 a.u., $\nabla^2\rho$ = 0.037 a.u., H = 0.0011 a.u., ε = 0.086, also at the B3LYP-D3(BJ)/def2-TZVP level of theory. In *cis*-1-naphthol, the low value of the electron density, the small positive value of the Laplacian, the values for ρ, $\nabla^2\rho$, and H for the H–H close-contact critical point are quite comparable to those of the weaker hydrogen bond in the acyclic formic acid dimer. The ellipticity, ε, though is relatively high in *cis*-1-naphthol, consistent with the close proximity of the ring and bond critical points. Bond and ring critical points move closer to each other as the dihedral angle τ is increased, indicating that the conformation becomes topologically unstable; at τ = 21° bond and ring critical points annihilate each other.

We find that the atomic energy, E_A, of the close-contact C-bonded H-atom in *cis*-1-naphthol is lower by 48.5 kJ mol^{-1} compared to the average energy of all other C-bonded H-atoms. In contrast, the same H-atom is higher in energy by 22.2 kJ mol^{-1} in *trans*-1-naphthol. The corresponding stabilization of the close-contact H-atoms in phenanthrene (total of 39.3 kJ mol^{-1}) has been interpreted by Bader and co-workers to be a result of a bonded interaction, *i.e.* H–H bonding.[22] The total H-atom energy is lower by 29.3 kJ mol^{-1} in *cis*-1-naphthol and the total heavy atom energy is higher by 33.9 kJ mol^{-1} than in *trans*-1-naphthol, consistent with what Bader and coworkers found for the phenanthrene/anthracene case, for example. In total, *trans*-1-naphthol is more stable by 4.6 kJ mol^{-1}, consistent with the theoretical calculations. A compilation of relevant data from the AIMAll calculations is in Table S18 of the ESI.†

The interpretation by Bader and co-workers of the bond path and bond critical point between the close-contact H-atoms in terms of bonding, *i.e.* H–H bonding, interactions has been criticized, for example by Bickelhaupt and co-workers.[27] In particular, they point out that the physical meaning of the atomic energy, E_A, is not particularly clear. They consider that the reduction of the H-atom E_A when two H-atoms come into close contact may be a result of mainly a reduction in atomic basin volume, for the case of insignificant charge transfer. Grimme *et al.*[26] have also voiced their doubts about interpreting the bond critical point between the close-contact H-atoms in terms of a bonding interaction. They analysed the experimental splitting between symmetric and antisymmetric stretching normal modes of vibration involving close-contact D-atoms in dideuteriophenantrene. From this analysis and by comparison with theoretical calculations, they conclude that the observations are inconsistent with a bonding interaction between the close-contact D-atoms. See also the rebuttal by Bader.[24]

Cremer, Kraka *et al.* introduced a new aromaticity delocalization index assessing π-delocalization in aromatic systems based on vibrational frequencies.[78,79] They could clarify that the larger stability of phenanthrene relative to anthracene predominantly results from its higher resonance energy, a direct consequence of the topology of ring annellation and not from a maximum electron density path between the bay H atoms.[78] Furthermore, they pointed out that the close spatial

proximity of ring and bond critical points in the bay region of phenanthrene and their low electron densities, as well as the positive energy density at the bond critical point, are indicative of an electrostatic, destabilizing interaction, confirming the findings of Grimme *et al.*[26]

(b) IGM analyses. To obtain more quantitative insights into the bond strengths within 1-naphthol, we carried out independent gradient model (IGM) analyses.[31–33] The intrinsic bond strength index (IBSI) is based on the δg descriptor of the IGM approach and was recently introduced by Klein *et al.*[34] A particular strength of the IGM approach is the ability to isolate and characterize interactions between pairs of atoms (or between fragments). The IBSI values are related to the bond strength and was shown that there is a good linear correlation between IBSI values and the corresponding local force constants. Weak interactions have IBSI values $\lesssim 0.15$ and for stronger or covalent interactions IBSI $\gtrsim$ 0.15.

The IBSI value for the close-contact H–H interaction in *cis*-1-naphthol is 0.031. Those for the hydrogen bond and for the O–H bond in the hydrogen bond acceptor molecule in the water dimer are 0.059 and 1.394, respectively, and for the strong and weak hydrogen bonds in the acyclic formic acid dimer 0.091 and 0.020, respectively.

To understand how the bonding situation in 1-naphthol evolves with dihedral angle τ, we determined IBSI values for all bonds, except the C–H bonds not involved in the H–H close contact, as function of τ. Fig. 3 displays the IBSI value corresponding to the close-contact H–H interaction and the sum of all IBSI values of all bonds involving only heavy atom as function of τ. The latter gives us an indication of the aggregate bond strength of the heavy atom skeleton as τ is varied. As anticipated, the H–H IBSI value decreases as τ increases. The aggregate IBSI value for the heavy atom skeleton decreases initially, indicating a destabilization as τ increases. This can be interpreted as a destabilization of a π-electron resonance structure as the π-electron delocalization into the C–O bond is hindered as the dihedral is increased. Once the OH H-atom begins to move to the *trans*-side, the aggregate heavy atom skeleton IBSI value increases again and reaches a slightly higher value at 180° than at 0°.

(c) Local mode analyses. An in-depth assessment of the O–H bond strengths can provide important indicators about the nature of the C–H···H–O interaction in *cis*-1-naphthol. The power relationship between BSO n and k^a of O–H bonds in naphthol and some reference molecules are shown in Fig. 4 and their respective local mode force constants and local mode frequencies are reported in Table S25 of the ESI.† In case of 1-naphthol, a bonding interaction between H-atoms would lead to a weakening of the O–H bond for the *cis* conformer compared to the *trans* conformer as electron density is moved from the O–H bond region. Conversely, a stronger O–H bond in *cis*-1-naphthol would be consistent with the traditional notion of a steric repulsion between the H-atoms. In comparison to the reference molecules, it can be seen that the O–H bond strengths in naphthol compounds tend to be weaker than those in water, propen-2-ol, and methanol while they are comparable to those in phenol and 2-propanol. Importantly, it is revealed that the O–H bond strengths in naphthol compounds vary in the order, *cis*-1-naphthol > *trans*-2-naphthol > *trans*-1-naphthol > *cis*-2-naphthol. This supports a mainly repulsive H–H interaction in *cis*-1-naphthol and contradicts the possibility of a dominant bonding interaction as one would speculate based on the bond critical point between the H-atoms. This observed trend in the O–H bond strengths for the naphthol compounds can also be visualized as a blue shift in the IR spectrum provided that the OH normal mode is not coupling with the other modes,

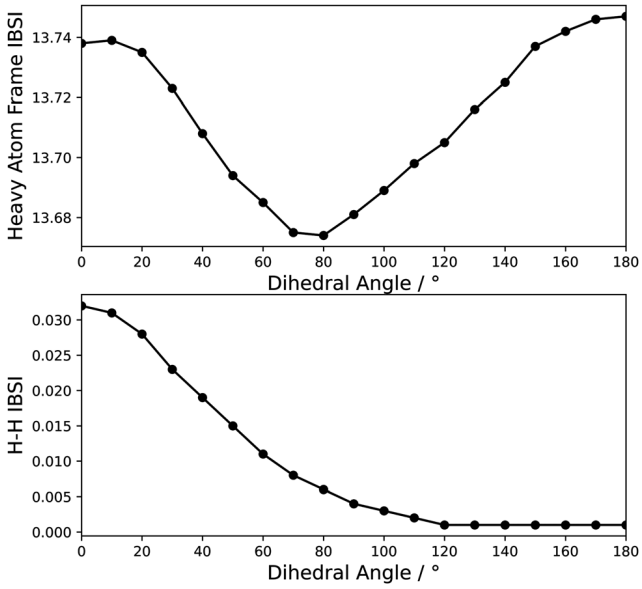

Fig. 3 Intrinsic bond strength indexes (IBSI), obtained from the independent gradient model (IGM) analysis, for the sum of the bonds in the heavy atom frame (top) and bonds participating in the close-contact H–H interaction (bottom) as a function of dihedral angle. The dihedral angle corresponds to the rotation of the hydroxyl group out of the ring plane.

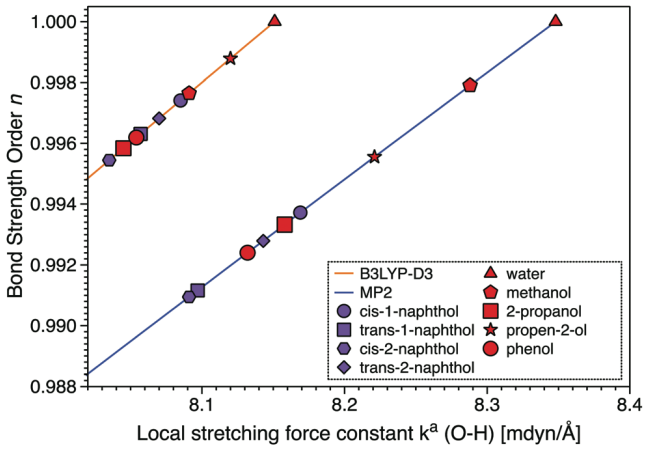

Fig. 4 Power relationship between bond strength order (BSO) n and k^a of O–H bonds in *cis*- and *trans*-, 1- and 2-naphthol (in purple) and reference molecules (in red) for B3LYP-D3(BJ) (orange line) and MP2 (blue line) calculations. (BSO) n has been scaled by a factor of 1.045 and 1.041 for B3LYP-D3(BJ) and MP2 calculations, respectively.

e.g., bending modes. We investigated this *via* the characterization of normal modes (CNM) procedure for *cis* and *trans* conformers of 1-naphthol calculated at the B3LYP-D3(BJ) level of theory. In Fig. S5 and S6 of the ESI,† the decomposition plots for all normal modes (51 modes) into a non-redundant set of 51 local modes, for *cis*- and *trans*-conformers of 1-naphthol, are shown where the OH normal mode is highlighted in yellow. It is observed that the OH normal stretching mode (3817 cm^{-1}) in the *cis* conformer has 99.9% contribution from O–H local stretching mode with up to 0.06% contributions from the two O–C–C local bending modes. Also, in the *trans* conformer, the O–H local stretching mode dominates with 99.93% contribution to the OH normal mode (3804 cm^{-1}). As the O–H normal modes in both conformers possess the character of an almost pure O–H stretching mode, one can directly compare the corresponding O–H normal modes. Thus, as reflected by the blue shift, which has also been confirmed experimentally,[15] of *cis*-1-naphthol we can quantify the repulsive aspect of the close-contact H-atoms based on vibrational spectroscopy.

(d) CM5 atomic charge analysis. In an effort to build on the previous methods discussed herein and further examine the interaction between the two close-contact H-atoms, a Charge Model 5 (CM5)[41] charge analysis was carried out, which derives partial atomic charges from a Hirshfeld population analysis. By measuring the CM5 atomic charges as the dihedral angle τ of *cis*-1-naphthol is varied from 90° to 0°, one can ultimately infer how the electron density around each atom changes as the two hydrogens approach each other. Because of the absence of a bond critical point (QTAIM and NCI plot in Fig. 2 and Fig. S3 of the ESI,† respectively) between the two hydrogens, we used *trans*-1-naphthol, *cis*-2-naphthol, and *trans*-2-naphthol as control molecules. We examined the charges of the five atoms which play the most prominent role in this interaction: the hydroxyl hydrogen (H′), oxygen (O′), the carbon bound to the oxygen (C′), the close-contact hydrogen (H″), and the carbon bound to the close-contact hydrogen (C″). The labelling is summarized in Fig. S13 of the ESI.† The charge as a function of dihedral angle for all four isomers of naphthol, and the net charge change for each atom are summarized in Fig. S14 and Table S30 of the ESI,† respectively. Based on Fig. S14 and Table S30 (ESI†), no anomalies are observed for atoms C″ and C′ of *cis*-1-naphthol as the charge change generally follows the same pattern as in the other isomers. For the most part the O′ atom follows the trends of the other isomers, with the net change (Table S30, ESI†) only slightly smaller than in its counterparts. Interestingly, for the two hydrogens the charge pattern for *cis*-1-naphthol deviates significantly from the other isomers. For the H″ atom the charge, and thus the electron density at the atom, does not change significantly in *cis*-1-naphthol, while the electron density decreases for the other isomers with increasing dihedral angle. For the H′ atom the charge decreases (increasing electron density) as the dihedral angle approaches 0°, while it stays almost constant for the other isomers. Although there is a clear increase in electron density for H′, attributing this to a bonding or non-bonding interaction is not so straightforward. On one hand the slightly smaller change in net charge of O′, and therefore less electron density being moved away from the O′ atom, may indicate a steric repulsive H–H interaction. On the other hand, an increase in electron density for the H′ atom may be indicative of a bonding interaction as electron density is being transferred to the H′ atom from the H″ atom.

(e) NBO analysis. To further examine this electron transfer and clarify the CM5 results, a Natural Bond Orbital (NBO) analysis[42,43] was carried out. We are extending a previous analysis[21] to provide a more comprehensive breakdown of the close-contact H–H interaction into its respective stabilization and steric exchange energies. An NBO analysis allows for the decomposition of non-covalent and covalent interactions into localized bonding and antibonding orbitals. In the framework of NBO an intermolecular interaction, or an intramolecular interaction as considered here, can be considered a charge transfer interaction where electron density is transferred from a bonding orbital (BD) at the donor site to an antibonding orbital (BD*) on the acceptor site. For example, if a bonding interaction was to be present in *cis*-1-naphthol one would observe an electron density transfer from the O′–H′ BD to the C″–H″ BD* and/or from the C″–H″ BD to the O′–H′ BD*. Table S31 of the ESI,† presents the electron occupancies for the O′–H′ BD, C″–H″ BD, O′–H′ BD*, and the C″–H″ BD*. From Table S31 (ESI†), there is a slightly lower occupancy in both the O′–H′ BD and C″–H″ BD and a higher occupancy in both the O′–H′ BD* and C″–H″ BD* in *cis*-1-naphthol compared to the other isomers, supporting the notion of a bonding interaction. Using a second order perturbative treatment of the Fock matrix, the two interactions (C″–H″ BD $\cdots$ O′–H′ BD* and O′–H′ BD $\cdots$ C″–H″ BD*) can be quantified in terms of stabilization energies as a function of dihedral angle τ (Tables S32–S35, ESI†). The sum of the two BD–BD* interactions for the close-contact H–H interaction is plotted in Fig. 5 for each isomer. The total summed donor–acceptor interactions for 1-naphthol with the close-contact H–H interaction subtracted from the total energy is shown in Fig. S16 of the ESI.† From Fig. 5 one can clearly see that the stabilization energies are several kJ mol^{-1} higher for *cis*-1-naphthol than for the other isomers, suggesting an attractive interaction between the two hydrogen atoms. To examine the repulsive components of the close-contact hydrogens we looked at the pairwise steric exchange energies between the C″–H″ BD and O′–H′ BD. The results are also plotted in Fig. 5. The total steric exchange energy with the close-contact H–H interaction subtracted from the total steric exchange energy is presented in Fig. S16 of the ESI.† The steric exchange energy for *cis*-1-naphthol increases far more compared to the other isomers as the dihedral angle approaches 0° and outweighs the stabilization energy by a factor of almost 3. The ωB97XD/Jun-cc-pVTZ results are also consistent with these findings, see Table S36 of the ESI.† Therefore, a large steric or repulsive interaction between the two hydrogens is present. Finally, comparing the steric (repulsion) energies to the stabilization (attraction) energies (Fig. 5) one can clearly see that although the stabilization energy is considerably larger compared to the other isomers, the steric energy is even larger and outweighs the stabilization contribution.

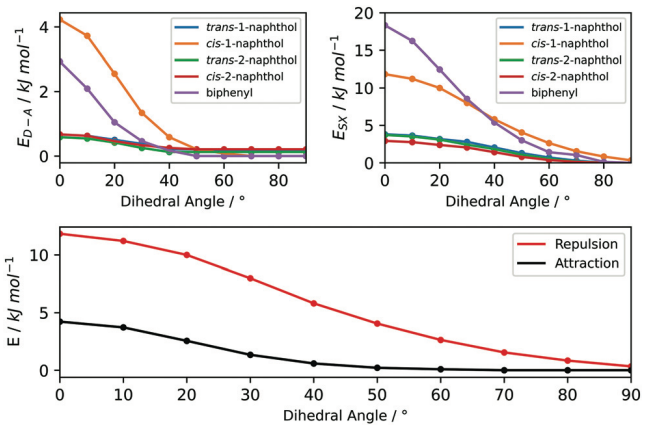

Fig. 5 Summed donor–acceptor (attraction) energies for the O–H bonding orbital (BD) ⋯ C–H antibonding orbital (BD*) and C–H BD ⋯ O–H BD* interactions (top left). Pairwise steric exchange (repulsion) energies between the C–H BD and O–H BD (top right). Comparison between the repulsive and attractive energies for *cis*-1-naphthol (bottom).

After these analyses, a coherent, albeit qualitative, picture of the close-contact H–H interaction emerges. At the equilibrium structure, there are no net forces acting on the atoms and therefore the repulsive forces between the two close-contact H atoms must be compensated for by bonding or some restoring forces. The topology of the electron density between the two close H-atoms, resembles, at least qualitatively, that of a weak hydrogen bond and it is difficult not to ascribe some bonding, *i.e.* stabilizing, character to it. This, however, appears not to be the dominant stabilizing interaction; that role we attribute to the resistance of the heavy atom skeleton to be forced out of one of its π-electron resonance structures. The role of maximizing the π-electron delocalisation in stabilizing the close H–H contact in *cis*-1-naphthol has already been pointed out by Whitham *et al.*[20]

Biphenyl: a related system

It is desirable to confirm the findings about the close-contact H–H interaction in *cis*-1-naphthol by comparing with similar systems. It is, however, difficult to find an analogue molecular system and we use biphenyl for comparison. Biphenyl has a soft coordinate, *i.e.* the phenyl–phenyl rotation, along which the H–H separation can be varied, similar to the OH rotation coordinate in *cis*-1-naphthol. Upon rotation by 180°, however, biphenyl assumes its original configuration and conversion to a conformer without close H–H contact, as in 1-naphthol, is not possible. Analogous to *cis*-1-naphthol, the single bond connecting the aromatic rings in biphenyl also exhibits a partial π character, thus hindering the rotation about that bond. As found previously,[22,80] biphenyl contains a BCP between two close-contact hydrogens in its planar geometry, which, much like *cis*-1-naphthol, annihilates with the corresponding RCP at $\tau \approx 22°$. Its equilibrium geometry is ≈40° out of plane. Fig. S4 of the ESI,† presents the results from an NCI analysis of the planar and equilibrium geometries of biphenyl. Just as with *cis*-1-naphthol, the planar geometry exhibits strong attraction between two pairs of similarly charged hydrogens, indicated by the blue colouration. This attraction is diminished in the equilibrium structure, consistent with the annihilation of the BCP with the RCP at ≈22°. Fig. 5 and Fig. S15 of the ESI,† present the NBO and CM5 results for the close-contact H–H atoms, respectively. The CM5 results for biphenyl differ somewhat from those of *cis*-1-naphthol where the atomic CM5 charge change is not as drastic in biphenyl (see Table S30 of the ESI†). The biphenyl NBO results are analogous to *cis*-1-naphthol, that is the donor–acceptor energy is relatively large when the two hydrogen atoms are in close contact, indicating an attraction, with the steric exchange energy also large when in close contact. In addition, the biphenyl close-contact case has a weaker attraction component and a stronger steric component than *cis*-1-naphthol, suggesting that the H–H interaction is actually stronger and more favourable in *cis*-1-naphthol than in biphenyl.

Despite the similarities between the two systems there is one underlying issue with biphenyl. Unlike *cis*-1-naphthol, where a BCP is present in the equilibrium geometry, the equilibrium geometry in biphenyl does not have a BCP between the close-contact hydrogen atoms; the close-contact H–H interaction is strongest in the planar geometry which is actually a transition state and not an equilibrium structure. Ultimately, the steric repulsion in biphenyl outcompetes the attractive component of the H–H interaction and the restoring force of the heavy atom frame, a result of the rotation about the partial π bond. This is in contrast with *cis*-1-naphthol where the steric repulsion of the two hydrogen atoms cannot overcome the combination of the attraction component and restoring force of the heavy atom skeleton.

Conclusions

Rotational spectra of the 1-naphthol and 2-naphthol monomers were recorded using a CP-FTMW spectrometer in the 2–6 GHz range. We assigned the spectrum of *trans*-2-naphthol and extended the measurements for the other isomers. In addition to the parent species, spectra of ten ^{13}C isotopologues were assigned for each conformer. The ^{13}C isotopologues were then used to determine carbon-skeleton substitution structures. The corresponding bond lengths and bond angles are in good agreement with the theoretical results.

For *cis*-1-naphthol, QTAIM and NCI analyses of the B3LYP-D3(BJ)/def2-TZVP calculated electron density give a bond path with bond critical point between the close-contact OH and ring H-atom. The IGM analysis reveals that the heavy atom skeleton aids in stabilizing the close-contact hydrogens, where the stabilizing force originates from the steric strain provided by the weakening of the π-electron delocalization. Local mode analyses were carried out for the naphthols and the O–H bond strengths were compared for all four conformers. The results show that *cis*-1-naphthol has the strongest O–H bond among the four isomers. This is consistent with the traditional notion of a steric repulsion between the two close-contact H-atoms, in accord also with the blue-shift of the OH stretching frequency in *cis*-1-naphthol. Charge Model 5 and, in particular, Natural

Bond Orbital analyses of *cis*-1-naphthol do support the notion of a weak bonding H–H interaction, which, however, is outweighed by steric repulsion. The major part of the stabilizing force is presumably provided by a maximization of π-electron delocalization, as already pointed out by Whitham *et al.*[20] In the flexible comparison molecule biphenyl, the steric repulsion of the two close-contact hydrogens outcompetes the attraction and heavy atom skeleton restoring force, in contrast with *cis*-1-naphthol, and the BCP disappears in the non-planar equilibrium structure.

The idea of a non-bonding or bonding H–H interaction has been previously met with controversy, with both camps presenting arguments for their conclusions. However, much like categorizing non-covalent interactions as either weak or strong, labelling the close-contact H–H interaction in *cis*-1-naphthol as purely non-bonding/repulsive or bonding/attractive does perhaps not give the whole picture. As presented with the several methods completed herein, close-contact H–H interactions involve a mixture of attractive and repulsive forces, with contributions from both the close-contact hydrogens and the heavy atom skeleton. Although there is an attractive component in the close-contact H–H interaction, it is overwhelmed by the repulsive component.

Conflicts of interest

There are no conflicts to declare.

Acknowledgements

We thank two anonymous referees for their constructive comments. This research was funded by the University of Alberta and the Natural Sciences and Engineering Research Council (NSERC) of Canada. We gratefully acknowledge access to the computing facilities of the Shared Hierarchical Academic Research Computing Network (SHARCNET: www.sharcnet.ca), the Western Canada Research Grid (Westgrid) and Compute/Calcul Canada. SN and EK thank the Center for Research Computing at Southern Methodist University for providing generous computational resources and the National Science Foundation for support (grant CHE 1464906).

Notes and references

1 H. Shindy, *Chem. Int.*, 2016, **2**, 2016.
2 C. Sams, *Toxics*, 2017, **5**, 3.
3 D. L. Sudakin, D. L. Stone and L. Power, *Curr. Top. Toxicol.*, 2011, **7**, 13.
4 R. Knochenmuss and S. Leutwyler, *J. Chem. Phys.*, 1989, **91**, 1268–1278.
5 T. Droz, R. Knochenmuss and S. Leutwyler, *J. Chem. Phys.*, 1990, **93**, 4520–4532.
6 S. Maity, R. Knochenmuss, C. Holzer, G. Féraud, J. Frey, W. Klopper and S. Leutwyler, *J. Chem. Phys.*, 2016, **145**, 164304.
7 S. Maity, P. Ottiger, F. A. Balmer, R. Knochenmuss and S. Leutwyler, *J. Chem. Phys.*, 2016, **145**, 244314.
8 R. Knochenmuss, S. Maity, F. Balmer, C. Müller and S. Leutwyler, *J. Chem. Phys.*, 2018, **149**, 034306.
9 R. Knochenmuss, R. K. Sinha and S. Leutwyler, *J. Chem. Phys.*, 2018, **148**, 134302.
10 M. Schütz, T. Bürgi, S. Leutwyler and T. Fischer, *J. Chem. Phys.*, 1993, **99**, 1469–1481.
11 C. Wickleder, D. Henseler and S. Leutwyler, *J. Chem. Phys.*, 2002, **116**, 1850–1857.
12 R. Knochenmuss, R. K. Sinha, A. Poblotzki, T. Den and S. Leutwyler, *J. Chem. Phys.*, 2018, **149**, 204311.
13 R. Knochenmuss, R. K. Sinha and S. Leutwyler, *J. Chem. Phys.*, 2019, **150**, 234303.
14 R. Yoshino, K. Hashimoto, T. Omi, S. Ishiuchi and M. Fujii, *J. Phys. Chem. A*, 1998, **102**, 6227–6233.
15 R. D. Knochenmuss and D. E. Smith, *J. Chem. Phys.*, 1994, **101**, 7327–7336.
16 S. J. Humphrey and D. W. Pratt, *J. Chem. Phys.*, 1996, **104**, 8332–8340.
17 M. Saeki, S. Ishiuchi, M. Sakai and M. Fujii, *J. Phys. Chem. A*, 2007, **111**, 1001–1005.
18 N. A. Seifert, A. S. Hazrah and W. Jäger, *J. Phys. Chem. Lett.*, 2019, **10**, 2836–2841.
19 J. R. Johnson, K. D. Jordan, D. F. Plusquellic and D. W. Pratt, *J. Chem. Phys.*, 1990, **93**, 2258–2273.
20 C. J. Whitham, R. J. Jackson and J. M. Brown, *J. Mol. Spectrosc.*, 1999, **195**, 172–176.
21 M. Goubet, M.-A. Martin-Drumel, F. Réal, V. Vallet and O. Pirali, *J. Phys. Chem. A*, 2020, **124**, 4484–4495.
22 C. F. Matta, J. Hernández-Trujillo, T.-H. Tang and R. F. Bader, *Chem. – Eur. J.*, 2003, **9**, 1940–1951.
23 C. F. Matta, *Hydrogen Bonding—New Insights*, Springer, 2006, pp. 337–375.
24 R. F. Bader, *J. Phys. Chem. A*, 2009, **113**, 10391–10396.
25 N. K. Monteiro and C. L. Firme, *J. Phys. Chem. A*, 2014, **118**, 1730–1740.
26 S. Grimme, C. Mück-Lichtenfeld, G. Erker, G. Kehr, H. Wang, H. Beckers and H. Willner, *Angew. Chem., Int. Ed.*, 2009, **48**, 2592–2595.
27 J. Poater, M. Solà and F. M. Bickelhaupt, *Chem. – Eur. J.*, 2006, **12**, 2889–2895.
28 J. Kraitchman, *Am. J. Phys.*, 1953, **21**, 17–24.
29 R. F. W. Bader, *Chem. Rev.*, 1991, **91**, 893–928.
30 E. R. Johnson, S. Keinan, P. Mori-Sánchez, J. Contreras-García, A. J. Cohen and W. Yang, *J. Am. Chem. Soc.*, 2010, **132**, 6498–6506.
31 C. Lefebvre, G. Rubez, H. Khartabil, J.-C. Boisson, J. Contreras-García and E. Hénon, *Phys. Chem. Chem. Phys.*, 2017, **19**, 17928–17936.
32 C. Lefebvre, H. Khartabil, J.-C. Boisson, J. Contreras-García, J.-P. Piquemal and E. Hénon, *Chem. Phys. Chem.*, 2018, **19**, 724–735.
33 M. Ponce-Vargas, C. Lefebvre, J.-C. Boisson and E. Hénon, *J. Chem. Inf. Model.*, 2020, **60**, 268–278.
34 J. Klein, H. Khartabil, J.-C. Boisson, J. Contreras-García, J.-P. Piquemal and E. Hénon, *J. Phys. Chem. A*, 2020, **124**, 1850–1860.

35 E. Kraka, W. Zou and Y. Tao, *Wiley Interdiscip. Rev.: Comput. Mol. Sci.*, 2020, **10**, e1480.
36 Z. Konkoli and D. Cremer, *Int. J. Quantum Chem.*, 1998, **67**, 1–9.
37 Z. Konkoli and D. Cremer, *Int. J. Quantum Chem.*, 1998, **67**, 29–40.
38 Z. Konkoli, J. A. Larsson and D. Cremer, *Int. J. Quantum Chem.*, 1998, **67**, 11–27.
39 E. Kraka, J. A. Larsson and D. Cremer, in *Computational Spectroscopy: Methods, Experiments and Applications*, ed. J. Grunenberg, Wiley N. Y., NY USA, 2010, pp. 105–149.
40 D. Cremer, J. A. Larsson and E. Kraka, *Theoretical and Computational Chemistry*, Elsevier, 1998, vol. 5, pp. 259–327.
41 A. V. Marenich, S. V. Jerome, C. J. Cramer and D. G. Truhlar, *J. Chem. Theory Comput.*, 2012, **8**, 527–541.
42 E. D. Glendening, C. R. Landis and F. Weinhold, *J. Comput. Chem.*, 2013, **34**, 1429–1437.
43 A. E. Reed and F. Weinhold, *J. Chem. Phys.*, 1983, **78**, 4066–4073.
44 W. Kohn and L. J. Sham, *Phys. Rev.*, 1965, **140**, A1133.
45 M. J. Frisch, G. W. Trucks, H. B. Schlegel, G. E. Scuseria, M. A. Robb, J. R. Cheeseman, G. Scalmani, V. Barone, G. A. Petersson, H. Nakatsuji, X. Li, M. Caricato, A. V. Marenich, J. Bloino, B. G. Janesko, R. Gomperts, B. Mennucci, H. P. Hratchian, J. V. Ortiz, A. F. Izmaylov, J. L. Sonnenberg, D. Williams-Young, F. Ding, F. Lipparini, F. Egidi, J. Goings, B. Peng, A. Petrone, T. Henderson, D. Ranasinghe, V. G. Zakrzewski, J. Gao, N. Rega, G. Zheng, W. Liang, M. Hada, M. Ehara, K. Toyota, R. Fukuda, J. Hasegawa, M. Ishida, T. Nakajima, Y. Honda, O. Kitao, H. Nakai, T. Vreven, K. Throssell, J. A. Montgomery Jr., J. E. Peralta, F. Ogliaro, M. J. Bearpark, J. J. Heyd, E. N. Brothers, K. N. Kudin, V. N. Staroverov, T. A. Keith, R. Kobayashi, J. Normand, K. Raghavachari, A. P. Rendell, J. C. Burant, S. S. Iyengar, J. Tomasi, M. Cossi, J. M. Millam, M. Klene, C. Adamo, R. Cammi, J. W. Ochterski, R. L. Martin, K. Morokuma, O. Farkas, J. B. Foresman and D. J. Fox, *Gaussian 16*, Gaussian Inc., Wallingford, CT, 2016.
46 S. Grimme, S. Ehrlich and L. Goerigk, *J. Comput. Chem.*, 2011, **32**, 1456–1465.
47 A. D. Becke, *J. Chem. Phys.*, 1992, **96**, 2155–2160.
48 A. D. Becke and E. R. Johnson, *J. Chem. Phys.*, 2005, **123**, 154101.
49 F. Weigend and R. Ahlrichs, *Phys. Chem. Chem. Phys.*, 2005, **7**, 3297–3305.
50 Ch. Møller and M. S. Plesset, *Phys. Rev.*, 1934, **46**, 618–622.
51 T. A. Keith, *AIMALL*, TK Gristmill Software, Overland Park, KS, 2017.
52 T. Lu and F. Chen, *J. Comput. Chem.*, 2012, **33**, 580–592.
53 E. F. Pettersen, T. D. Goddard, C. C. Huang, G. S. Couch, D. M. Greenblatt, E. C. Meng and T. E. Ferrin, *J. Comput. Chem.*, 2004, **25**, 1605–1612.
54 W. Zou, Y. Tao, M. Freindorf, M. Z. Makoś, N. Verma, D. Cremer and E. Kraka, Local Vibrational Mode Analysis (LModeA), *Computational and Theoretical Chemistry Group (CATCO)*, Southern Methodist University, Dallas, TX, USA, 2021.
55 E. B. Wilson, J. C. Decius and P. C. Cross, *Molecular vibrations: the theory of infrared and Raman vibrational spectra*, Courier Corporation, 1980.
56 W. Zou and D. Cremer, *Chem. – Eur. J.*, 2016, **22**, 4087–4097.
57 S. Nanayakkara, Y. Tao and E. Kraka, *J. Chem. Theory Comput.*, 2022, **18**, 562–579.
58 M. Freindorf and E. Kraka, *J. Mol. Model.*, 2020, **26**, 1–15.
59 S. Yannacone, M. Freindorf, Y. Tao, W. Zou and E. Kraka, *Crystals*, 2020, **10**, 556.
60 A. A. Delgado, D. Sethio, I. Munar, V. Aviyente and E. Kraka, *J. Chem. Phys.*, 2020, **153**, 224303.
61 W. Zou, R. Kalescky, E. Kraka and D. Cremer, *J. Chem. Phys.*, 2012, **137**, 084114.
62 N. Verma, Y. Tao, W. Zou, X. Chen, X. Chen, M. Freindorf and E. Kraka, *Sensors*, 2020, **20**, 2358.
63 R. M. Badger, *J. Chem. Phys.*, 1934, **2**, 128–131.
64 G. G. Brown, B. C. Dian, K. O. Douglass, S. M. Geyer, S. T. Shipman and B. H. Pate, *Rev. Sci. Instrum.*, 2008, **79**, 053103.
65 N. A. Seifert, J. Thomas, W. Jäger and Y. Xu, *Phys. Chem. Chem. Phys.*, 2018, **20**, 27630–27637.
66 H. M. Pickett, *J. Mol. Spectrosc.*, 1991, **148**, 371–377.
67 R. D. Chirico, W. V. Steele and A. F. Kazakov, *J. Chem. Thermodyn.*, 2015, **86**, 106–115.
68 D. Schemmel and M. Schütz, *J. Chem. Phys.*, 2008, **129**, 034301.
69 J.-D. Chai and M. Head-Gordon, *Phys. Chem. Chem. Phys.*, 2008, **10**, 6615–6620.
70 E. Papajak, J. Zheng, X. Xu, H. R. Leverentz and D. G. Truhlar, *J. Chem. Theory Comput.*, 2011, **7**, 3027–3034.
71 P. Pulay, W. Meyer and J. E. Boggs, *J. Chem. Phys.*, 1978, **68**, 5077–5085.
72 F. Pawłowski, P. Jørgensen, J. Olsen, F. Hegelund, T. Helgaker, J. Gauss, K. L. Bak and J. F. Stanton, *J. Chem. Phys.*, 2002, **116**, 6482–6496.
73 M. Piccardo, E. Penocchio, C. Puzzarini, M. Biczysko and V. Barone, *J. Phys. Chem. A*, 2015, **119**, 2058–2082.
74 M. K. Jahn, J.-U. Grabow, M. J. Travers, D. Wachsmuth, P. D. Godfrey and D. McNaughton, *Phys. Chem. Chem. Phys.*, 2017, **19**, 8970–8976.
75 T. Oka, *J. Mol. Struct.*, 1995, **352**, 225–233.
76 P. L. A. Popelier, F. M. Aicken and S. E. O'Brien, *Atoms in molecules*, Prentice Hall, Manchester, 2000.
77 V. Tognetti and L. Joubert, *J. Phys. Chem. A*, 2011, **115**, 5505–5515.
78 R. Kalescky, E. Kraka and D. Cremer, *J. Phys. Chem. A*, 2014, **118**, 223–237.
79 D. Setiawan, E. Kraka and D. Cremer, *J. Org. Chem.*, 2016, **81**, 9669–9686.
80 J. Cioslowski and S. T. Mixon, *J. Am. Chem. Soc.*, 1992, **114**, 4382–4387.

